Journal of Electronics, Electromedical Engineering, and Medical Informatics
Homepage: jeeemi.org; Vol. 7, No. 4, October 2025, pp: 330-340 e-ISSN: 2656-8632

RESEARCH ARTICLE OPEN ACCESS

BRU-SOAT: Brain Tissue Segmentation via Deep Learning-based Sailfish Optimization and Dual Attention SegNet

Athur Shaik Ali Gousia Banu[1], **Sumit Hazra**[2]

[1] Research Scholar, Department of Computer Science and Engineering, Koneru Lakshmiah Education Foundation, Hyderabad, 500075, Telangana, India. (Reg. no: 2312031051)
[2] Assistant Professor, Department of Computer Science and Engineering, Koneru Lakshmiah Education Foundation, Hyderabad, 500075, Telangana, India.

Corresponding author: Athur Shaik Ali Gousia Banu. (e-mail: gbanuzia@gmail.com), **Author(s) Email**: Sumit Hazra (sumit.hazra@klh.edu.in)

Abstract **Automated segmentation of brain tissue into gray matter (GM), white matter (WM), and cerebrospinal fluid (CSF) from magnetic resonance imaging (MRI) plays a crucial role in diagnosing neurological disorders such as Alzheimer's disease, epilepsy, and multiple sclerosis. A key challenge in brain tissue segmentation (BTS) is accurately distinguishing boundaries between GM, WM, and CSF due to intensity overlaps and noise in the MRI image. To overcome these challenges, we propose a novel deep learning-based BRU-SOAT model for BTS using the BrainWeb dataset. Initially, brain MRI images are fed into skull stripping to remove skull regions, followed by preprocessing with a Contrast Stretching Adaptive Wiener (CSAW) filter to improve image quality and reduce noise. The pre-processed images are fed into ResEfficientNet for fine feature extraction. After extracting the features, the Sailfish Optimization (SFO) is employed to select the most related features while eliminating irrelevant features. A Dual Attention SegNet (DAS-Net) segments GM, CSF, and WM with high precision. The proposed BRU-SOAT model is assessed based on its precision, F1 score, specificity, recall, accuracy, Jaccard Index, and Dice Index. The proposed BRU-SOAT model achieved a segmentation accuracy of 99.17% for brain tissue segmentation. Moreover, the proposed DAS-Net outperformed fuzzy c-means clustering, fuzzy consensus clustering, and U-Net methods, achieving 98.50% (CSF), 98.63% (GM), and 99.15% (WM), indicating improved segmentation accuracy. In conclusion, the BRU-SOAT model provides a robust and highly accurate framework for automated brain tissue segmentation, supporting improved clinical diagnosis and neuroimaging analysis.**

Keywords **Brain tissue segmentation, ResEfficientNet, Sailfish Optimization, Deep learning, Dual Attention SegNet**.

I. Introduction

Segmentation of brain images is a vital procedure in both clinical diagnosis and basic neuroscience research [1], [2]. Brain image segmentation involves estimating a labeled image that categorizes anatomical and structural regions based on MRI scans [3], [4]. In addition to providing a quantitative assessment of brain tissue volume, segmentation allows objective analysis and research, reducing reliance on visual inspection by experts [5]. MRI is a powerful tool for studying brain structures and functions, driving growing interest in assessing both child and adult brain development [6]. MRI provides multiple cross-sectional views of the brain with varying contrasts, enabling noninvasive and safe brain examination [7].

As a result of deep learning (DL), automatic segmentation methods are more accurate and faster than traditional methods [8], [9]. DL methods enable accurate extraction of regions of interest in the brain and differentiation from normal tissue, facilitating precise quantitative analysis [10]. Accurate segmentation of WM, GM, and CSF is crucial in clinical and neuroscience studies for analyzing brain structures, diagnosing neurological disorders, and monitoring disease progression [11], [12]. With DL-based segmentation, anatomical structures can be visualized and analyzed, surgical planning can be facilitated, and image-guided interventions can be supported. In recent years, DL has gained popularity for segmenting medical images [13]. DL-based techniques have also made significant progress in segmenting brain tissueacross adults, infants, and fetuses [14]. Despite these advances, BTS still faces numerous difficulties due to intricacy and intensity fluctuations of brain MRI. It is now difficult to accurately

Manuscript received March 29, 2024; Revised August 10, 2025; Accepted September 5, 2025; date of publication September 8, 2025
Digital Object Identifier (**DOI**): https://doi.org/10.35882/jeeemi.v7i4.795

segment MR images in order to diagnose and treat patients more successfully [15].

Accurate MRI-based BTS remains challenging due to complex image architecture, intensity variations, limited training data, and influencing factors such as imaging parameters, noise, and artifacts, which impact model generalizability and segmentation accuracy. To address these challenges, a novel DL-based model, BRU-SOAT, has been proposed for accurate brain tissue segmentation. The following are the BRU-SOAT model's primary contributions.

1. Initially, the skull regions are removed from the brain MRI images through skull stripping, and a CSAW filter is applied for preprocesses the images to enhance image and reduce noise.
2. A hybrid model combining EfficientNet compound scaling and ResNet residual connections is employed to extract complex features from MRI images.
3. SFO is used to select the most relevant features while preserving critical information to enhance segmentation accuracy.
4. The selected features are fed into the DAS-Net, which employs an encoder-decoder structure to segment brain tissues (WM, GM, CSF) with high precision.

The structure of the paper is planned as follows: Section-2 defines the literature survey; Section 3 describes the proposed BRU-SOAT model ; Section 4 and Section 5 report the performance analysis and experimental results , followed by a discussion. The work is concluded in Section 6.

II. Literature Survey

Several studies have recently achieved BTS using DL approaches. The following section briefly discusses a few recent research papers.

In 2023, Lee, J. et al. [16] suggested a framework for dividing the head-brain and fine-level stroke-affected areas in both chronic stroke patients and normal controls. According to the experiment's findings, the suggested approach outperforms traditional DL-based segmentation model across assessment criteria. However, one limitation of the study is that the framework may not generalize well to diverse populations due to limited dataset variability. Lai, Z. et al. [17] proposed an automatic segmentation technique in 2022 to remove tissue artifacts. It evaluates segmentation masks using Grad-CAM and offers relevant explanations and insights. While effective, the method relies on Grad-CAM for interpretability, which may provide coarse and less precise localization of important features.

Also in 2022, Rao, V.M. et al., [18] proposed a CNN–Transformer hybrid architecture that leverages the enhanced performance and generalization capabilities of Transformers for 3D medical picture segmentation applications to enhance BTS. And it demonstrates the model's dependability using test-retest scans conducted at various times. One limitation is that domain variability may degrade the model's performance when applied to medical images from different scanners or institutions. An adaptation strategy for improving brain tissues to separate WM, GM, and CSF tissues was proposed by Veluchamy, M. et al. in 2021 [19]. Experiment results show that the suggested approach strikes a decent balance between noise and intensity inhomogeneity. The method may struggle with accurate tissue separation in regions with severe intensity overlap or low contrast between tissues. By developing a membership function derived from a voting schema, Aruna Kumar, S.V. et al. [20] proposed a fuzzy consensus clustering technique in 2022 to cluster the pixels. It uses a number of segmentation algorithms based on intuitionistic and conventional fuzzy sets. The method may suffer from increased computational complexity due to the integration of multiple fuzzy-based segmentation algorithms

The WM, GM, and CSF were separated from newborn MR images using a subject-specific atlas-based approach proposed by Mhlanga, S.T. et al. in 2023 [21]. BTS is done by the expectation maximization Markov random field approach, atlas selection is done, and subject-specific atlases are created using the random forest (RF) classifier. The accuracy of this segmentation heavily depends on the quality and representativeness of the subject-specific atlases. A multi-branch CNN with attention modulation was proposed by Fan, X. et al. in 2022 [22] for the purpose of segmenting neonatal brain tissue. The proposed network features multiple attention modules in the decoding path and multi-scale convolutions in the encoding path. The proposed method has increased computational complexity due to multiple attention modules and multi-scale convolutions. Wu, C. et al. [23] proposed a GNN-SEG-based method for BTS in 2022. GNN-SEG uses GNNs to learn the topology of brain tissues using super pixels as basic processing units. GNN-SEG's performance may be limited by its reliance on accurate superpixel generation, which can affect segmentation quality in complex brain structures. From this literature, the existing technique works exhibit several limitations on BTS using different ML and DL models. A major challenge in BTS is ensuring model adaptability to variations in MRI scanners, acquisition protocols, and patient populations, which can significantly impact accuracy and reliability in clinical applications.

Manuscript received March 29, 2024; Revised August 10, 2025; Accepted September 5, 2025; date of publication September 8, 2025
Digital Object Identifier (**DOI**): https://doi.org/10.35882/jeeemi.v7i4.795

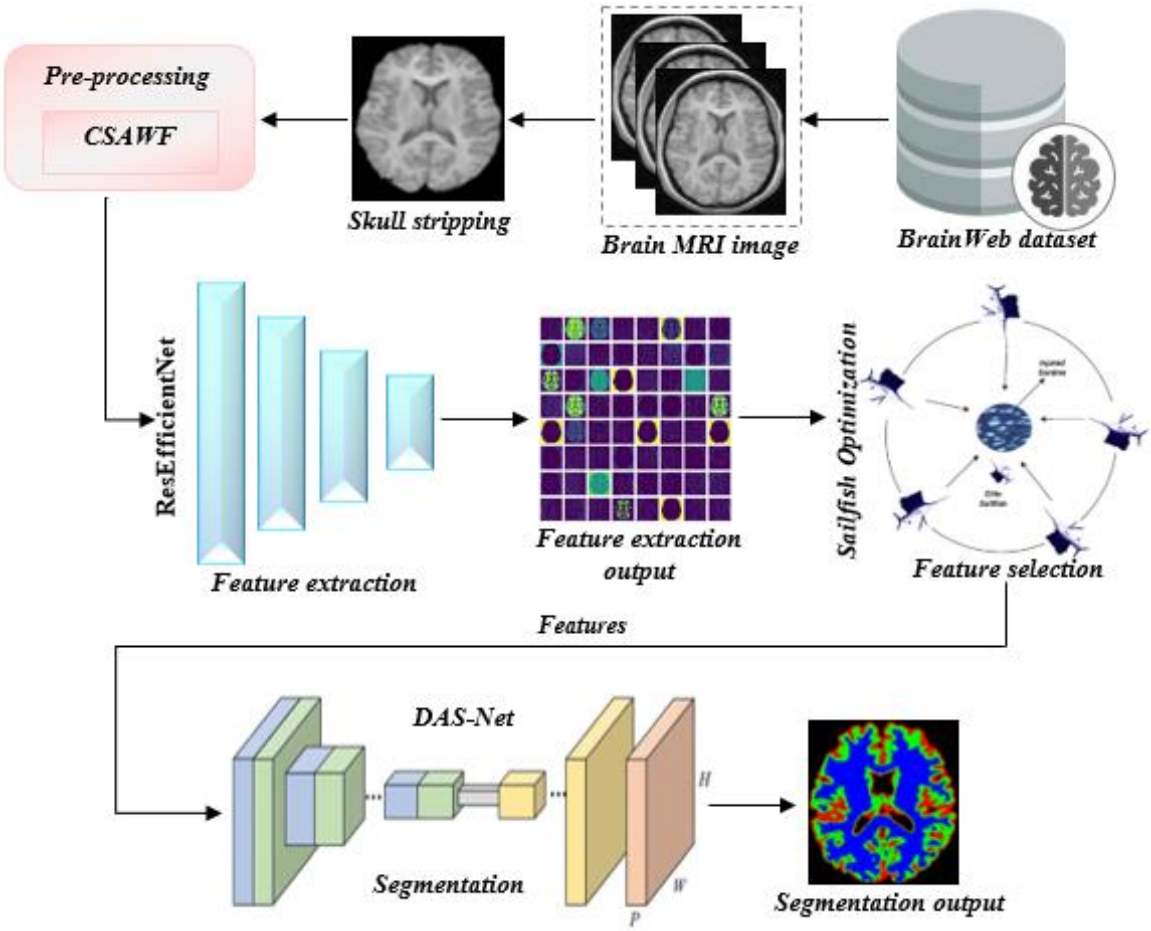

Fig. 1. Proposed BRU-SOAT methodology

Another key challenge in BTS is accurately distinguishing boundaries between GM, WM, and CSF due to intensity overlaps and noise in the MRI image. To overcome these problems, a novel BRU-SOAT was introduced for the accurate segmentation of brain tissues.

III. Proposed BRU-SOAT Methodology

A. Dataset Description

Brain MRI scans were sourced from the BrainWeb dataset [24]. The popular synthetic MRI dataset BrainWeb provides controlled situations with different intensity non-uniformities and noise levels. The dataset includes varying noise levels and RF inhomogeneity levels to simulate intensity non-uniformities and enhance model robustness. There are 36 images in a training set from all noise levels and RF levels, 12 in a validation set, and 57 in a test set.

B. Pre-Processing

In the pre-processing phase, initially, skull stripping is performed. The skull stripping process involves thresholding, morphological operations, and mask

In this research, BRU-SOAT is proposed for BTS using MRI images. The CSAW filter preprocesses the input images to enhance tissue contrast and reduce noise. ResEfficientNet extracts the complex features, and SFO is applied for feature selection to select the most related features. A DAS-Net is used to segment the brain tissues with high precision. Fig. 1 displays the proposed BRU-SOAT methodology.

application. This process increases the signal-to-noise ratio and reduces feature ambiguity for downstream learning models. After stripping the skull from the input MRI image then the images are pre-processed by CSAWF is combined by two filters, namely Contrast Stretching (CS) and Adaptive Wiener (AW) filter. CS is used to improve the image quality, and AW is used to preserve edges and fine structures while reducing noise and artifacts.

1. Contrast Stretching: In this denoising phase, every original intensity value is replaced, and the comparison of histograms is conducted through a locally modified contrast-stretching adjustment. A flexible transfer function, based on the input image characteristics, is used to assign a new level to each pixel Eq (1) [25].

Manuscript received March 29, 2024; Revised August 10, 2025; Accepted September 5, 2025; date of publication September 8, 2025
Digital Object Identifier (**DOI**): https://doi.org/10.35882/jeeemi.v7i4.795

$$Range = |Q_{max-}Q_{min}| \quad (1)$$

Where, $X_k$is the new intensity value assigned to the pixel at position k after processing, $Q_N$is the current pixel intensity value in the input image and σ_N is the scaling factor applied to smooth the intensity transitions. Here Q_{max} and Q_{min} are the input image's maximum and minimum values for the new intensity. Currently, each pixel equation is given an additional intensity by Eq (2), Eq (3) [25],

$$X_k = \begin{cases} Q_{N-}\sigma_N & ,if\ Q_N = Q_{max} \\ Q_{N+}\sigma_N & ,if\ Q_N = Q_{min} \end{cases} \quad (2)$$

$$r_n = M - \sqrt{(range - M)^2} \quad (3)$$

Here, r_n is the normalized range factor. Every pixel value is altered using the previously given formulas, where M is the Intensity range normalization Falls between 0.01 and 0.02.

2. Adaptive Wiener filter: In order to decrease the mean square error between the original and restored images, it adapts the filter output to the local variance of the image. This approach is especially effective in preserving edges and high-frequency regions, offering a more powerful filtering effect compared to other techniques. On the one hand, it employs a large number of window settings to manage different situations and automatically choose the best one. To lessen subjectively annoying singularities, the center sample in the moving window was ignored in smooth sections but used correctly in rough ones. The problem with filtering signal-intendent noise-contaminated images could be shown Eq (4) [26]:

$$y(i,j) = x(i,j) + n(i,j) \quad (4)$$

The objective is to denoise y (i, j), where n (i, j) represents the additive noise and x (i, j) is the original noise-free image. To achieve this, multiple window sizes $(3 + 2i)^2$, with i = 0, 1, 2, 3 … are evaluated based on the pixel's mean and variance, and the window with the highest average value is selected for final processing. The region can be used to adaptively choose the filter template. Efficiency is increased while preserving borders and texture elements by using a big window filter in the smooth area and a tiny window filter in the detail section. The pixels are processed using the Eq (5), Eq (6), Eq (7) [26] formula to produce the desired outcome.

$$r(i,j) = \mu + (1 - q + \Delta) * (s(i,j) - \mu \quad (5)$$

$$q = \frac{\sigma_{avg}}{\sigma_{var}+1} \quad (6)$$

$$\Delta = \frac{\sigma_{var}}{\sigma_{avg}+\sigma_{max}+1} \quad (7)$$

In The symbols s (i, j) represent the original pixel, r (i, j) the output pixel, q represents the scaling factor based on local and average variance, Δ represents the modulation factor calculated from variances. σ_{var} defines the current pixel, μ denotes the Mean intensity of the local window centered at (i,j), σ_{max} for the image's highest variance over all pixels, and σ_{avg} represents the average of the variance values computed across all pixels within the selected window. These steps enhance tissue contrast, suppress noise and artifacts, and preserve spatial detail, thereby refining the accuracy and efficiency of subsequent feature extraction.

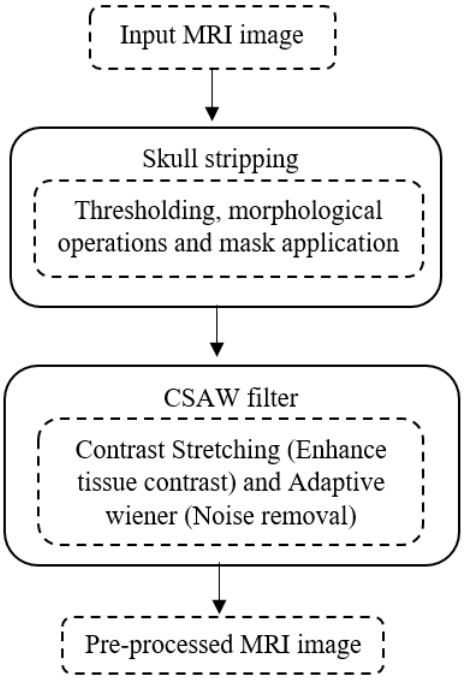

Fig. 2. Flowchart of the proposed BRU-SOAT model for MRI Image Pre-processing

Fig. 2 illustrates the MRI image pre-processing pipeline. It includes skull stripping using thresholding, morphological operations, and mask application, followed by CSAW filtering for noise removal and tissue contrast enhancement.

Data augmentation techniques like rotations, flips, intensity variations, and zoom scaling improve model generalization by addressing orientation, contrast, and anatomical size differences, making them essential for learning robust features from the limited BrainWeb dataset.

C. Feature Extraction

ResEfficientNet is a hybrid architecture that combines the ResNet [27] and EfficientNet [28] to extract complex features from MRI images. It typically merges the residual connections of ResNet with the MBConv blocks and compound scaling of EfficientNet. ResEfficientNet enables efficient, deep, and multi-scale feature extraction with low computational cost, improved gradient flow, and strong generalization across diverse MRI datasets. Fig. 3 shows the ResEfficientNet architecture. A CNN with 101 layers is

Manuscript received March 29, 2024; Revised August 10, 2025; Accepted September 5, 2025; date of publication September 8, 2025
Digital Object Identifier (**DOI**): https://doi.org/10.35882/jeeemi.v7i4.795

called a residual network (ResNet-101V2). The vanishing gradient issue is intended to be resolved by ResNet-101V2 [29]. ResNet-101V2 introduces the concepts of residual blocks and skip connections. By omitting a few layers in the center, the skip connection links layers with other levels. If a layer causes performance degradation, it can be skipped using the skip connection. The residual blocks are combined to create ResNet. This model is well-known for its residual connections and deep architecture, which aid in the multi-layer learning of complicated characteristics. ResNet-101V2 is beneficial for recognizing texture variations in high-intensity images since it is especially good at maintaining features across many levels and identifying small details. Using a set of predefined coefficients, the compound scaling technique EfficientNet adjusts the network's breadth, length, and resolution. Each layer's feature maps are increased by scaling the width. The network's layers rise as scaling depth increases. The resolution of input images is increased through scaling. EfficientNetB0 is highly suited for the task of feature extraction due to its compound scaling technique, which aids in capturing both large-scale and fine-grained information relating to shape and texture.

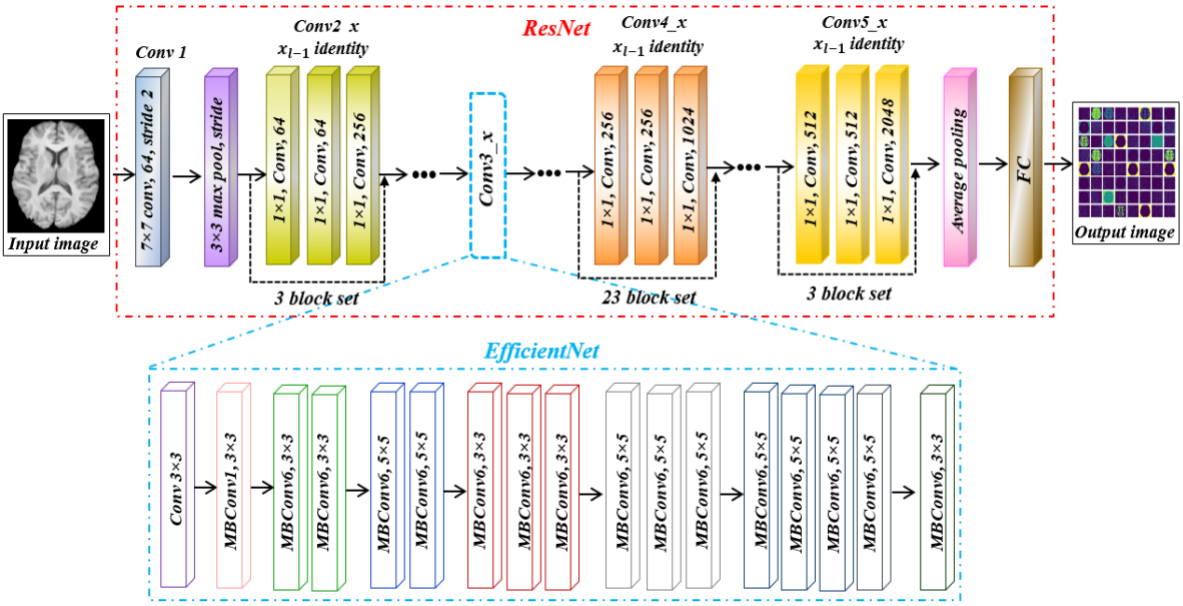

Fig. 3. ResEfficientNet architecture

D. Feature Selection

For feature selection, the SFO [30] algorithm is used. It mimics the hunting strategy of sailfish and sardines, balancing exploration and exploitation through population dynamics. In this study, the fitness function used by the SFO algorithm was defined as the classification accuracy achieved on a validation set after applying the selected features to the DAS-Net segmentation model. The goal was to maximize segmentation accuracy while minimizing the number of selected features, thereby preserving only the most informative features for downstream processing. In the algorithm, the sailfish and sardine population are generated randomly as follows Eq (8) [30]:

$$AP = AP_{max} - iter \times \frac{AP_{max} - AP_{min}}{MaxIter} \quad (8)$$

Where AP is Attack Power parameter, $iter$ is the current iteration, $MaxIter$ is the iterations of maximum number and AP_{max}, AP_{min} are predefined limits. Fitness values of each sailfish and sardine are calculated and stored in matrices. The best sailfish and sardine are known as elite sailfish and injured sardine, respectively Eq (9) [30]:

$$Elite = argmin_i f(X_i), \quad Injured = \arg max_j f(X_j) \quad (9)$$

Where X_i denotes the position of the ith sailfish in the population, X_j represents the position of the jth sailfish in the population, f(X) denotes the fitness function, $argmin_i f(X_i)$ represents the index i of the sailfish whose position X_i has the minimum fitness value, $\arg max_j f(X_j)$ represents the index j of the sailfish whose position Y_i has the maximum fitness value, elite denotes the best individual in the population, and Injured refers to the worst individual in the population. Sailfishes replace their position based on both the elite one and the injured sardine Eq (10) [30]:

$$X_i^{new} = X_i + AP \times (Elite - X_i) + (1 - AP)(InjuredX_i) \quad (10)$$

Where, X_i^{new} denotes the revised location of the ith candidate solution in the search space for the next

Manuscript received March 29, 2024; Revised August 10, 2025; Accepted September 5, 2025; date of publication September 8, 2025
Digital Object Identifier (**DOI**): https://doi.org/10.35882/jeeemi.v7i4.795

iteration. $AP \times (Elite - X_i)$ directs the sailfish towards the elite sailfish, exploiting the best solution found so far, and $(1 - AP) \times (Injured - X_i)$ incorporates exploration by considering the injured sardine, helping to maintain diversity and avoid optima. Sardine update their positions based on the attack power of the sailfish. All sardines modify their positions if attack power is greater than 0.5; otherwise, the number of sardines that are proportional to attack power just redirect their position Eq (11) [30].

$$X_j^{new} = \begin{cases} X_j + AP \times (Elite - X_j), & AP > 0.5 \\ X_j + rand() \times (Elite - X_j), & AP \leq 0.5 \end{cases} \quad (11)$$

Where, X_j^{new} denotes updated position of the jth sardine (individual) in the population after position adjustment, X_j represents the current position of the jth sardine, rand() defines the random number between 0 and 1, and AP denotes the attack power parameter. When, AP> 0.5 all sardines move towards the elite sailfish, ensuring a stronger convergence towards optimal solutions. When, AP≤ 0.5 only a fraction of the sardines adjust their positions, helping in exploration by maintaining diversity in the search space. Furthermore, in each iteration, elite sailfish and injured sardine are updated if a better one is observed. The position of a final elite sailfish is returned from the sailfish matrix and concludes the algorithm. The optimal number of features was determined by evaluating the trade-off between performance and feature count, using the elbow method on the performance curve. The SFO parameters were tuned experimentally and set as follows: population size = 30, maximum iterations = 50, and attack power threshold = 0.5. These values were chosen using a grid search strategy based on segmentation accuracy on the validation dataset. The final output of the SFO is the position of the elite sailfish, which corresponds to the most effective subset of features for BTS.

E. Segmentation

Using the DAS-Net model, the suggested approach accomplishes end-to-end pixel segmentation. For scene understanding applications that require efficient memory and processing time during inference, this semantic segmentation network was created. The three primary parts of SegNet [31] are a pixel-wise classification layer, a matching decoder block, and an encoder block. Similar to the VGG16 architecture, the SegNet generates a set of feature maps using a 13-convolutional-layer encoder. A 13-layer decoder network is produced by matching decoder layers for each encoder layer. Conversely, the decoder creates sparse feature maps by up-sampling feature maps that are sent into it. High-resolution feature maps can be preserved by the encoder by removing fully connected layers. A softmax classifier receives the final decoder output and uses rich feature representations to classify pixels. SegNet is therefore more time- and memory-efficient than other semantic segmentation designs since it has fewer trainable parameters. When the VGG16 model is initially constructed using pre-trained weights, the top levels, that is, the completely connected layers, are excluded.

1. Dual-attention module

Attention mechanisms are applied at different scales or levels of the SegNet architecture. This attention is applied to intermediate feature maps to emphasize important spatial locations during the segmentation process. The proposed method incorporates two attention mechanisms: spatial attention block (SAB) and channel attention block (CAB). SAB minimizes channel size by performing two convolutional layers and then sigmoid (SI) activation for each spatial pixel. In order to create a CAB, spatial size is decreased by means of global average pooling (GAP), then the SI is activated. The SAB and CAB are then multiplied point-wise with feature maps.

Spatial attention block (SAB). This includes improved focus on relevant spatial information, enhanced feature learning, and the ability to adaptively attend to different parts of the input data for better task performance. As a result of spatial attention, a spatial weight map (W_m) is learned based on correlations between spatial positions, which is then multiplied by the equivalent spatial locations to capture additional characteristic features. GAP and global max pooling (GMP) are performed at every spatial position to efficiently learn spatial weight connections, producing two feature descriptors. Concatenate these feature descriptors and manage them through a 7 × 7 convolution to crop the final spatial attention map in Eq. (12) [32].

$$W_m(C) = sigmoid\left(c^{7\times7}([Avgpool(C); Maxpool\ (C)])\right) \quad (12)$$

Where, $W_m(C)$ represents the resulting spatial attention map that highlights the importance of each spatial location in the feature map c, c denotes the Input feature map, sigmoid denotes the sigmoid activation function normalizes the output values between 0 and 1, $\mathrm{Avgpool(C)}$ represents an average pooling operation applied spatially on C, producing a summary of average activations at each spatial location, $Maxpool\ (C)$denotes max pooling operation applied spatially on C, capturing the strongest activations at each spatial location. where $c^{7\times7}$ signifies a convolution operation with 7 × 7 kernel size. This module generates a spatial attention map by considering the importance of each spatial location within the feature maps. The spatial attention mechanism is illustrated as Eq (13) [32],

$$M_s(f) = \sigma(f\left(f_j(f_{avg} + f_{max})\right)) \quad (13)$$

Manuscript received March 29, 2024; Revised August 10, 2025; Accepted September 5, 2025; date of publication September 8, 2025
Digital Object Identifier (**DOI**): https://doi.org/10.35882/jeeemi.v7i4.795

Where $M_s(f)$ is the resulting spatial attention map, which is of shape 1×H×W. This is applied element-wise to the input feature map to emphasize or suppress spatial locations. f is the input feature map and f_j is the join operation. By averaging the channel dimension and max pooling the kernel, a feature representation of size 2 × H × W is produced. f_{avg} is the average pooling and f_{max} is max pooling. σ is the sigmoid activation function, used to normalize the attention weights between 0 and 1. The following is the derivation of the entire computation process, Eq (14) [32].

$$fA = M_s(f)f' \; where \; f' = M_c(f)f \quad (14)$$

Where f' is the channel-attended feature, obtained by applying a channel attention map $Mc(f)$ to the input feature map f. $M_s(f)$ represents the spatial attention map derived from fA denotes the final attended feature map. The up-sampling block of VNet is inserted after the attention module, allowing this module to eliminate redundant features in both channel and spatial dimensions and concentrate on crucial features.

Channel attention block (CAB). A multichannel feature map $C = X^{ch \times ht \times wt}$ was created from a high-resolution image from remote sensing after it had passed through multiple convolutional layers, where $ht, ch,$ and wt specify the number the height, channels, and width of the feature. Every channel's feature map expresses information differently. The goal of channel attention is to multiply a 1D weight $W_{ch} \in X^{ch \times 1 \times 1}$ to the appropriate channel by using the relationships among each channel in the feature map. It was concentrated more on the semantic nuances pertinent to the current task to this strategy. To produce two feature descriptors per channel, GAP and GMP are first applied to the spatial dimensions. These descriptors are then utilized to learn an effective weight representation. To generate more representative feature vectors, both descriptors are fed through a shared multilayer perceptron (MLP) with a single hidden layer that contains C/8 units. The information in the resultant vectors is then concatenated by summing them element-by-element. Finally, an SI activation function is useful to obtain the CAB in Eq (15) [33].

$$W_{ch}(C) = sigmoid\big(MLP([Avgpool(C))\ MLP(Maxpool\ (C)])\big) \quad (15)$$

where $W_{ch}(C)$ Channel attention weights for the input C, same number of channels as input, values between 0 and 1. sigmoid is the Nonlinear activation function, MLP denotes the Multi-layer perceptron, AvgPool denotes the average pooling operation applied across the spatial dimensions of C, MaxPool refers to the max pooling operation applied similarly, capturing the strongest activations per channel. In order to learn the residual and enable faster convergence, a skip link is introduced straight from input to output, leaving the input and output channels unchanged. This module effectively captures and highlights important channel-wise information, enabling the model to adaptively focus on the related features. The final channel attention mechanism is illustrated as Eq (16) [33]:

$$P_c(f) = \sigma((w_1 w_0)f_{avg} + (w_1 w_0)f_{max}) \quad (16)$$

where $P_c(f)$ denotes the output of the function after applying weighted pooling and nonlinear activation on the input feature map f. w_i is the weight of layer i, σ is the nonlinear activation function, f is the input feature map, and f_{avg} and f_{max} are the results of the input f after the average pooling and kernel maximum pooling, respectively.

Table 1 demonstrates the parameters of the DAS-Net. A batch size of 16 and 100 training epochs, utilizing categorical cross-entropy loss and the Adam optimizer, are important hyperparameters for the DAS-Net model. It employs 3×3 convolutional filters and ReLU activation across 13 encoder-decoder layers. The attention modules use a 7×7 kernel in SAB and a C/8 hidden unit MLP in CAB to enhance spatial and channel-wise feature learning. Table 2 provides a hyperparameter of the proposed BRU-SOAT model components, including preprocessing with CSAW filtering, feature extraction using ResEfficientNet, feature selection via SFO, and segmentation with DAS-

Table 1. Training Parameters of DAS-Net

Hyperparameter	Value
Input image size	256 × 256
Number of convolutional layers	13 (VGG16-based)
Filter size (Conv layers)	3×3
Batch size	16
Loss function	Categorical Cross-Entropy
Stride	1
Pooling type	Max-pooling
Activation function	ReLU
Number of epochs	100
Optimizer	Adam
Attention kernel size (SAB)	7×7
MLP hidden units (CAB)	C/8

Manuscript received March 29, 2024; Revised August 10, 2025; Accepted September 5, 2025; date of publication September 8, 2025
Digital Object Identifier (**DOI**): https://doi.org/10.35882/jeeemi.v7i4.795

Table 2. Hyperparameters of BRU-SOAT model

Component	Hyperparameters	Values	Tuning Process
Pre-processing (CSAW Filter)	CS Range, AW Filter Window Size	0.01 - 0.02, multi-window sizes $(3+2i)^2$	Experimentally selected based on noise reduction and contrast enhancement results
Feature Extraction (ResEfficientNet)	Input Image Size, Number of Layers, Optimizer, Learning Rate	256×256, 101 Layers (ResNet-101V2), Adam, 0.001	Selected based on compound scaling and residual connections for deep features
Feature Selection (SFO)	Population Size, Max Iterations, Attack Power Threshold	30, 50, 0.5	Grid search strategy on validation set for best segmentation accuracy
Segmentation (DAS-Net)	Input Image Size, Convolutional Layers, Activation Function, Learning Rate, Batch Size, Loss Function, Attention Kernel Size (SAB), MLP Hidden Units (CAB)	256×256, 13 (VGG16-based), ReLU, 0.001, 16, Categorical Cross-Entropy, 7×7, C/8	Parameters were fine-tuned based on segmentation accuracy and stability over training epochs

Net. Each stage is optimized with specific hyperparameters such as learning rates, filter sizes, and population sizes selected through experimental tuning and grid search strategies. These configurations ensure enhanced noise reduction, effective feature extraction, optimal feature selection, and precise segmentation of brain tissues. The fine-tuned parameters significantly contribute to the proposed model's high accuracy and robustness in MRI BTS. Fig. 4 presents the workflow of the proposed BRU-SOAT model for BTS. The input MRI image undergoes skull stripping, contrast enhancement using a CS filter, and noise removal via an AW filter. ResNet and EfficientNet extract detailed and multi-scale features, respectively. SFO selects the most relevant features for accurate segmentation. Finally, DAS-Net segments brain tissues using spatial and channel attention mechanisms, producing the final segmented MRI image. A proposed BRU-SOAT model was assessed based on F1, RE, PR, SP, AC, DI, and JI. SP evaluates the model's accuracy in identifying negative situations. It is computed by separating the total number of negatives by the number of correctly predicted negatives. It is illustrated as Eq (17) [34]:

$$SP = \frac{T_{neg}}{T_{neg}+F_{pos}} \quad (17)$$

PR calculates the percentage of optimistic forecasts that come true. It emphasizes the model's ability to minimize false positives, which is illustrated as Eq (18) [35]:

$$PR = \frac{T_{pos}}{T_{pos}+F_{pos}} \quad (18)$$

RE evaluates the model's capacity to accurately detect every real positive case. It is the ratio of correctly predicted positive observations to all actual positives it is illustrated as Eq (19) [34]:

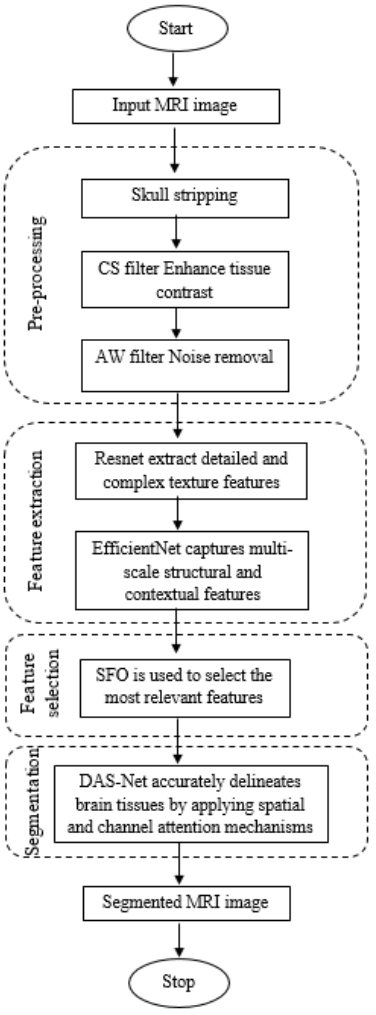

Fig. 4. Flowchart of the proposed BRU-SOAT model for BTS

Manuscript received March 29, 2024; Revised August 10, 2025; Accepted September 5, 2025; date of publication September 8, 2025
Digital Object Identifier (**DOI**): https://doi.org/10.35882/jeeemi.v7i4.795

The JI measures the similarity among two sets by

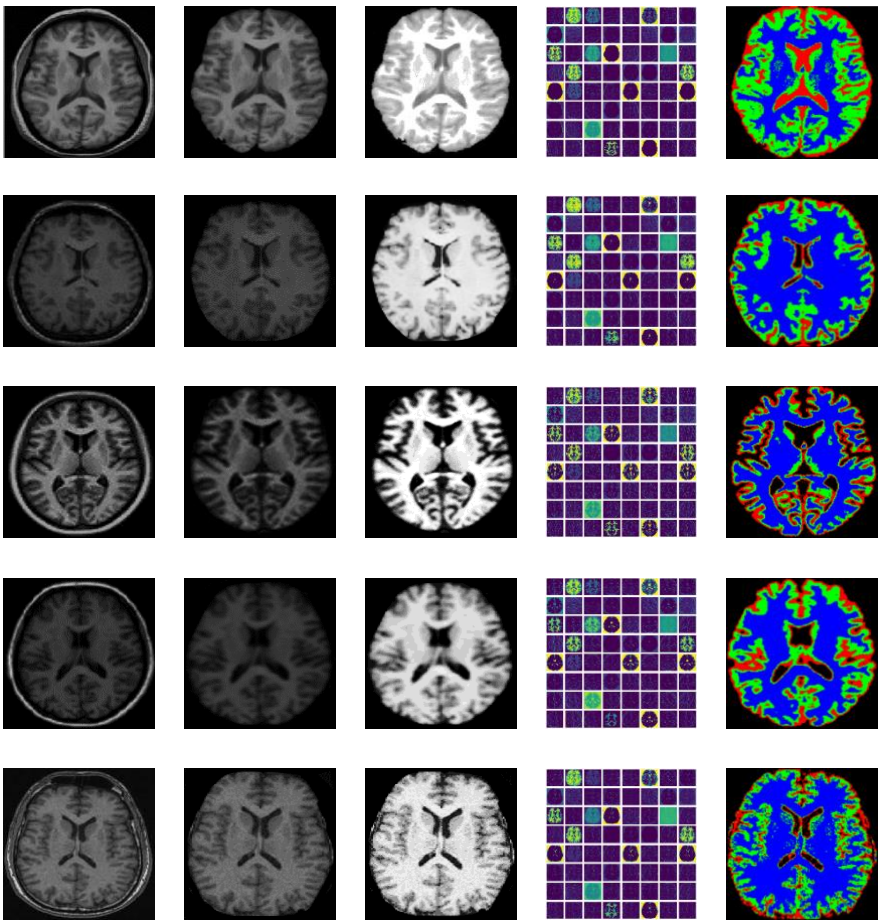

Fig. 5. Experimental result of the proposed BRU-SOAT (a) input image, (b) skull stripped image, (c) pre-processed image, (d) feature extracted image, (e) segmented image

$$RE = \frac{T_{pos}}{T_{pos}+F_{neg}} \quad (19)$$

AC calculates how accurate the model's predictions are overall. It is computed as the proportion of accurately predicted samples to all samples, it is illustrated as Eq (20) [34]:

$$AC = \frac{T_{pos}+T_{neg}}{Total\ no.of\ samples} \quad (20)$$

F1 represents the harmonic mean of PR and RE, offering a balanced measure. When there is an uneven class distribution, it is illustrated as Eq (21) [35]:

$$F1 = 2\left(\frac{Precision+Recall}{Precision+Recall}\right) \quad (21)$$

The DI is a similarity measure used to gauge the overlap between two sets, often used in image segmentation to compare the segmentation with the ground truth. It is illustrated as Eq (22) [34]:

$$DI = \frac{2T_{pos}}{F_{pos}+2T_{pos}+F_{neg}} \quad (22)$$

comparing the intersection over the union of the sets it is illustrated as Eq (23) [34]:

$$JI = \frac{T_{pos}}{T_{pos}+F_{neg}+F_{pos}} \quad (23)$$

where T_{neg} and T_{pos} specifies true negatives and true positives of the sample images, F_{neg} and F_{pos} requires false negatives and false positives of the sample images.

IV. Results

This section uses MATLAB 2019 b to implement the proposed model efficiency, a DL toolbox. The BRU-SOAT is assessed by various measures like accuracy (AC), specificity (SP), precision (P), recall (RE), Jaccard Index (JI), Dice Index (DI), and F1 score (F1). Benchmarks include the BRU-SOAT method's overall accuracy rates, performance explicitly specified and assessed. Fig. 5 demonstrates the simulation results of the proposed brain MRI processing pipeline using

Manuscript received March 29, 2024; Revised August 10, 2025; Accepted September 5, 2025; date of publication September 8, 2025
Digital Object Identifier (**DOI**): https://doi.org/10.35882/jeeemi.v7i4.795

Table 3. Performance assessment of the BRU-SOAT model

Types	AC	PR	RE	SP	F1
CSF	99.04	98.62	97.10	98.03	95.72
GM	98.63	97.84	96.72	98.66	98.14
WM	99.85	98.51	97.46	96.72	96.53

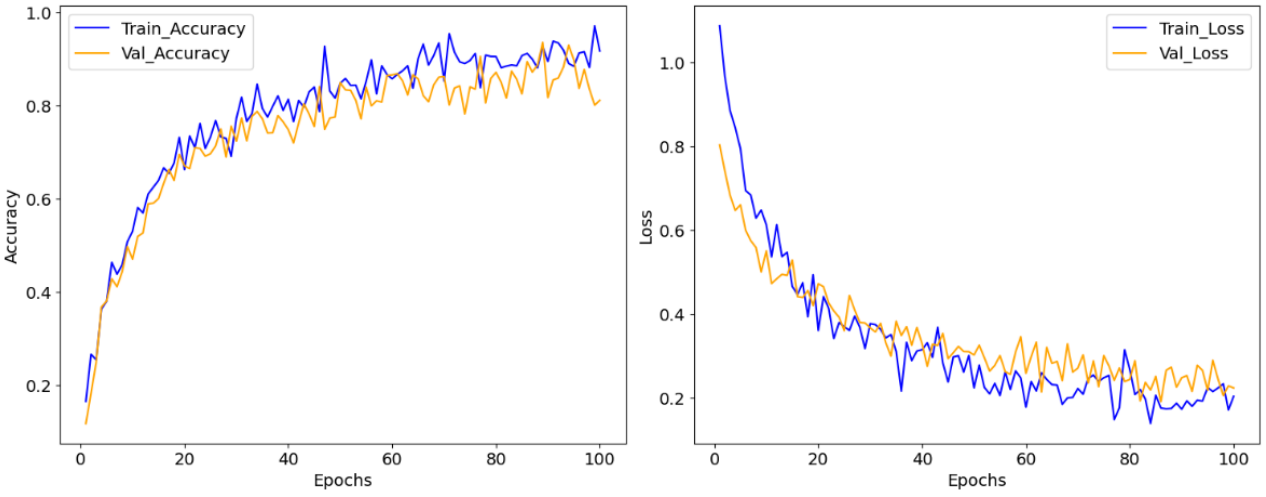

a) b)

Fig. 6. Performance evaluation of the proposed DAS-Net (a) accuracy graph and (b) loss graph

different input samples. Column 1 presents the original brain MRI scans, while Column 2 displays the Skull Stripping MRI images to remove non-brain tissues. Column 3 illustrates the pre-processed MRI scans, improving contrast and normalization for better feature extraction. Column 4 represents extracted feature maps highlighting significant patterns in the brain structure. Column 5 shows the final segmented outputs, and Table 3 displays the classification performance attained by the proposed BRU-SOAT model for BTS. A total accuracy of 99.17% is achieved by the proposed BRU-SOAT model on the dataset. The proposed BRU-SOAT model also achieves 98.32%, 96.79%, 97.80%, and 97.09% overall precision (PR), f1 score (F1), specificity (SP), and recall (RE). Fig. 6 a) and b) show the accuracy and loss graph of the suggested BRU-SOAT model. The accuracy curve is shown in Fig. 6a), where AC and epochs are positioned on opposite axes. The model's AC rises as the number of epochs grows. The epoch versus loss curve is shown in Fig. 6b), where the model's loss decreases as the number of epochs rises. The proposed BRU-SOAT model achieves an accuracy of 99.17%. The performance of the proposed BRU-SOAT was evaluated using 3-fold and 5-fold cross-validation to ensure the robustness and reliability of the BRU-SOAT framework. The dataset was split into respective folds, and the results were averaged across all runs with two different cross-validation methods, as illustrated in Table 4. Table 4 displays the cross-validation results of the BRU-SOAT model utilizing 3-fold and 5-fold cross-validation techniques. There are three subsets of the data in the 3-fold cross-validation. where 40% is used for training in each fold, and the remaining 20% is used for testing. The data is separated into five subgroups for the 5-fold cross-validation, with 20% of each subset being utilized for testing and 20% for training.

Table 4. Cross-validation results of the proposed model

Metric	3-Fold Cross-Validation	5-Fold Cross-Validation
AC	98.12%	98.21%
PR	97.83%	96.01%
RE	96.26%	96.09%
F1	98.05%	97.55%
SP	97.84%	96.10%

In this section, the experimental fallouts of the suggested BRU-SOAT are discussed by focusing on a comparison of its performance with other segmentation

Manuscript received March 29, 2024; Revised August 10, 2025; Accepted September 5, 2025; date of publication September 8, 2025
Digital Object Identifier (**DOI**): https://doi.org/10.35882/jeeemi.v7i4.795

Table 5. Comparison of Segmentation approaches

Methods	AC	JI	DI
Graphcut [36]	95.86	93.67	90.67
SegNet [37]	93.15	91.76	93.55
U-Net [38]	98.75	94.79	95.56
DAS-Net	99.17	97.91	98.76

methods. The segmentation metrics, such as the JI and DI, are used to assess the efficiency of each algorithm. These metrics help in understanding the precision and accuracy of the segmentation techniques in various scenarios. Table 5 illustrates the comparison of various segmentation algorithms with the DAS-Net based on DI and JI metrics. The proposed DAS-Net increases the overall DI by 8.9%, 5.56%, and 3.34 for Graphcut, SegNet, and U-Net, respectively. According to the Table.5, DAS-Net has the highest DI (98.76) and JI (97.91) scores among Graphcut, SegNet, and U-Net algorithms. From this analysis, the proposed DAS-Net indicates the best segmentation performance. Fig. 7 compares different methods for BTS in MRI images. The columns show the brain MRI, results from Graphcut, SegNet, U-Net, and DAS-Net. Graphcut produces noisy segmentations with boundary distortions, resulting in an estimated 35-40% loss in segmentation accuracy due to misclassified regions. SegNet and U-Net improve the results by reducing noise and better capturing structures, but they still show 15-20% inconsistencies in tissue differentiation compared to the ground truth. The DAS-Net achieves the best segmentation, preserving fine structural details with over 90% boundary accuracy, making it 10-15% better than U-Net and SegNet. This highlights the effectiveness of attention mechanisms in improving BTS quality.

The proposed ResEfficientNet with four DL classifiers, AlexNet [39], RegNet [40], GoogleNet [41], and MobileNet [42] were evaluated for competence. The accuracy accomplished by the suggested ResEfficientNet is 99.17%, which is better than the traditional DL networks. The proposed ResEfficientNet is higher than that of classic networks like AlexNet, RegNet, GoogleNet, and MobileNet. ResEfficientNet maintains a 99.17% high accuracy range. The proposed ResEfficientNet improves its accuracy by 5.89%, 2.04%, 1.15% and 5.04% better than AlexNet, RegNet, GoogleNet, and MobileNet, respectively. Table 6 compares the existing models with the proposed BRU-SOAT. The fuzzy c-means clustering method achieved the lowest DI values with 40.1% (CSF), 82.8% (GM), and 89.9% (WM). The fuzzy consensus clustering approach showed significant improvement, reaching 93.64% (CSF), 94.71% (GM), and 93.17% (WM). U-Net further improved segmentation with DI values of 91.2% (CSF), 94.5% (GM), and 94.7% (WM). The proposed BRU-SOAT outperformed all previous methods, achieving98.50%

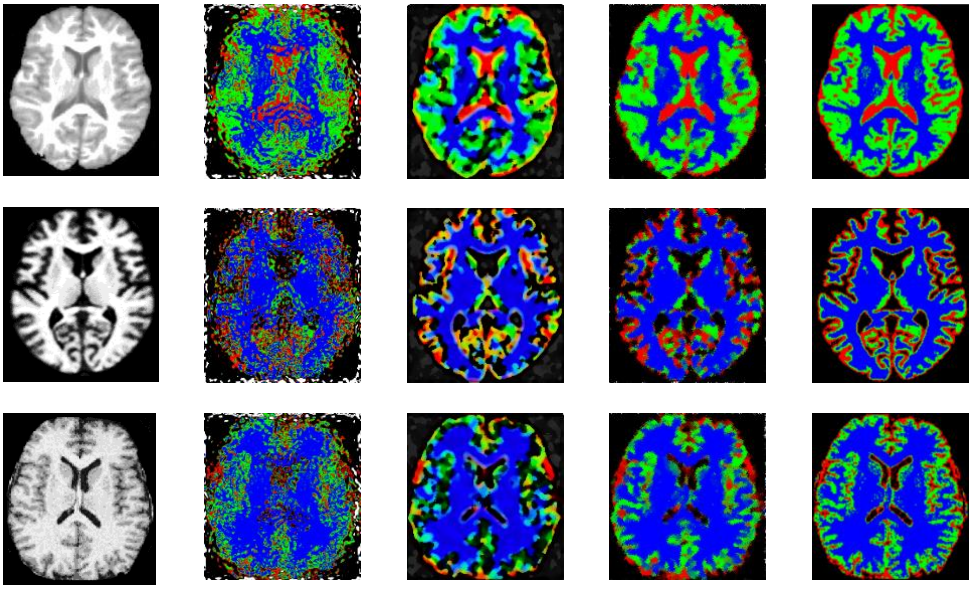

Fig. 7. Visualization results of different segmentation technique (a) input image, (b) Graphcut, (c) SegNet, (e) U-Net, and (e) DAS-Net.

Manuscript received March 29, 2024; Revised August 10, 2025; Accepted September 5, 2025; date of publication September 8, 2025
Digital Object Identifier (**DOI**): https://doi.org/10.35882/jeeemi.v7i4.795

(CSF), 98.63% (GM), and 99.15% (WM), demonstrating superior segmentation accuracy.

SegNet and U-Net are CNN-based models; among them, U-Net performs better due to the use of skip connections. The proposed DAS-Net uses attention mechanisms to focus on important tissue regions. DAS-Net achieves the highest accuracy and segmentation performance among all methods. GraphCut [36] achieves 95.86% accuracy and a DI of 90.67%. SegNet [37] has 93.15% accuracy and a DI of 93.55%. U-Net [38] performs better with 98.75% accuracy and a DI of 95.56%. The proposed DAS-Net outperforms all, achieving 99.17% accuracy and a DI of 98.76% (Table 5). It achieved an overall segmentation accuracy of 99.17%, with DI of 98.50% for CSF, 98.63% for GM, and 99.15% for WM 9 (Table 6). In contrast, conventional U-Net-based models typically report DI between 94–96% for these tissue types. Additionally, ablation studies confirmed that ResEfficientNet surpasses traditional feature extraction networks such as AlexNet, RegNet, GoogleNet, and MobileNet, underscoring its effectiveness in extracting meaningful spatial and textural information.

Table 6. Comparison of existing methods vs proposed BRU-SOAT

Authors	Methods	DI		
		CSF	GM	WM
Veluchamy, M. and Subramani, B., [19] (2021)	fuzzy c-means clustering algorithm	40.1%	82.8%	89.9%
Aruna Kumar, S.V et al, [20] (2022)	fuzzy consensus clustering algorithm	93.64%	94.71%	93.17%
Mhlanga, S.T. and Viriri, S., [21] (2023)	U-Net	91.2%	94.5%	94.7%
Proposed	BRU-SOAT	98.50%	98.63%	99.15%

V. Discussion

The BRU-SOAT model demonstrates a significant advancement in automated BTS by effectively tackling critical challenges such as intensity overlap, anatomical complexity, and MRI noise. The inclusion of CSAW filtering enhances image contrast and suppresses noise artifacts. ResEfficientNet, as the feature extraction backbone, enables the capture of fine-grained features for accurate segmentation. The application of the SFO algorithm ensures that only the most relevant features are retained, thereby minimizing computational burden and enhancing the model's ability to focus on important regions. Furthermore, the DAS-Net augmented with SAB and CAB directs the model's attention toward critical anatomical boundaries, significantly improving tissue delineation and classification accuracy. Table 4 presents the cross-validation results of the proposed model, showing consistent performance across both 3-fold and 5-fold validations. The model achieves a high accuracy of 98.21% and an F1 score of 97.55%, indicating robust and reliable segmentation capability. The proposed DAS-Net increases the overall DI by 8.9%, 5.56%, and 3.34% for Graphcut, SegNet, and U-Net Fig. 7.

The proposed ResEfficientNet improves its accuracy by 5.89%, 2.04%, 1.15% and 5.04% better than AlexNet, RegNet, GoogleNet, and MobileNet. The proposed BRU-SOAT model achieves 98.32%, 96.79%, 97.80%, and 97.09% overall precision, F1 score, specificity, and recall (Table 3). These improvements collectively demonstrate the robustness and clinical relevance of the BRU-SOAT model for accurate and efficient BTS. When evaluated segmentation methods like U-Net [38], GraphCut [36] and SegNet [37], the proposed BRU-SOAT model exhibits superior performance. GraphCut is a traditional method based on energy minimization but is sensitive to noise.

A limitation of this study lies in its reliance on the synthetic BrainWeb dataset, which does not fully replicate the variability, noise, and anatomical diversity present in real clinical MRI data. This may affect the model's generalizability to practical clinical environments. Furthermore, performance on multi-institutional, multi-modal data remains unexplored, which could impact robustness across imaging protocols and scanner types. Despite dataset-related limitations, the BRU-SOAT framework presents a robust and efficient solution for automated BTS. It sets a strong foundation for clinical-grade applications, offering potential benefits in early diagnosis and monitoring of neurodegenerative disorders, pre-surgical planning, and longitudinal patient assessments. Future work should focus on validating the model using real-world clinical datasets and exploring integration with multi-modal MRI to enhance adaptability and clinical relevance.

VI. Conclusion

Manuscript received March 29, 2024; Revised August 10, 2025; Accepted September 5, 2025; date of publication September 8, 2025
Digital Object Identifier (**DOI**): https://doi.org/10.35882/jeeemi.v7i4.795

This study aimed to develop a DL-based BRU-SOAT model for BTS using MRI images from the BrainWeb dataset. The primary goal was to overcome challenges such as noise, intensity overlap, and boundary ambiguity by integrating advanced preprocessing, feature extraction, and attention-based segmentation techniques. The main finding of this research is that the proposed BRU-SOAT model achieved a segmentation accuracy of 99.17%, significantly outperforming traditional methods. Class-wise segmentation accuracy using DAS-Net was 98.50% for CSF, 98.63% for GM, and 99.15% for WM. Additionally, ResEfficientNet improved feature extraction performance by 5.89%, 1.94%, 0.62%, and 3.17% compared to AlexNet, RegNet, GoogleNet, and MobileNet, respectively, demonstrating its superior discriminative capability. An additional finding is the effectiveness of incorporating SFO for feature selection, which helped in reducing redundant information and improving segmentation accuracy. Moreover, the integration of spatial and channel attention mechanisms in DAS-Net enabled the model to better focus on relevant anatomical regions, enhancing segmentation precision.

Acknowledgment

The author would like to express his heartfelt gratitude to the supervisor for his guidance and unwavering support during this research for his guidance and support.

Funding

Not applicable.

Data Availability

Data sharing does not apply to this article as no datasets were generated or analyzed during the current study.

Author Contribution

Athur Shaik Ali Gousia Banu conceptualized and designed the study, conducted data collection, and participated in data analysis and interpretation. Sumit Hazra contributed to the development of the educational media, oversaw the implementation of the intervention, and contributed to manuscript writing and revisions. Athur Shaik Ali Gousia Banu and Sumit Hazra assisted with data analysis and interpretation and provided critical feedback on the manuscript. All authors reviewed and approved the final version of the manuscript and agreed to be responsible for all aspects of the work, ensuring integrity and accuracy.

Declarations

Ethical Approval

My research guide reviewed and ethically approved this manuscript for publication in this Journal.

Consent for Publication Participants.

Not applicable.

Competing Interests

This paper has no conflict of interest for publication.

References

[1] J. R. F. Raj, K. Vijayalakshmi, S. K. Priya, and A. Appathurai, "Brain tumor segmentation based on kernel fuzzy c-means and penguin search optimization algorithm," *Signal, Image Video Processing*, vol. 18, no. 2, pp. 1793—1802, 2024.

[2] R. Sundarasekar, and A. Appathurai, "FMTM-feature-map-based transform model for brain image segmentation in tumor detection," *Network: Comput. Neural Systems*, vol. 34, no. 1--2, pp. 1-25, 2023.

[3] R. Abirami, and P. Krishna Kumar, "Deep Learning Model for Accurate Brain Tumor Detection Using CT and MRI Imaging," *International Journal of System Design and Computing*, vol. 02, no. 01, pp. 26-31, 2024.

[4] P.K. Mishro, S. Agrawal, R. Panda, L. Dora, and A. Abraham, "Intensity inhomogeneity correction in brain MRI: a systematic review of techniques, current trends and future challenges," *Neural Computing and Applications*, pp. 1-18, 2024.

[5] A. Appathurai, A. S. I. Tinu, and M. Narayanaperumal, "Meg and Pet Images-Based Brain Tumor Detection Using Kapur's Otsu Segmentation and Sooty Optimized Mobilenet Classification," *Revue Roumaine des Sciences Techniques—Série Électrotechnique Et Énergétique*, vol. 69, no. 3, pp. 359-364, 2024.

[6] Ghazanfar Ali Safdar, and Xiaochun Cheng, "Brain Aneurysm Classification Via Whale Optimized Dense Neural Network," *International Journal of Data Science and Artificial Intelligence*, vol. 02, no. 02, pp. 63-67, 2024.

[7] R. Sundarasekar, and A. Appathurai, "Efficient brain tumor detection and classification using magnetic resonance imaging," *Biomedical Physics Engineering Expression*, vol. 7, no. 5, pp. 055007, 2021.

[8] T. Kunkyab, Z. Bahrami, H. Zhang, Z. Liu, and D. Hyde, "A deep learning-based framework (Co-ReTr) for auto-segmentation of non-small cell-lung cancer in computed tomography images," *Journal of Applied Clinical Medical Physics*, vol. 25, no. 3, pp. e14297, 2024.

[9] V.K. Kanaujia, A. Kumar, and S.P. Yadav, "Advancements in Automatic Kidney Segmentation using Deep Learning Frameworks and Volumetric Segmentation Techniques for CT Imaging: A Review," *Archives of Computational Methods in Engineering*, pp. 1-19, 2024.

Manuscript received March 29, 2024; Revised August 10, 2025; Accepted September 5, 2025; date of publication September 8, 2025
Digital Object Identifier (**DOI**): https://doi.org/10.35882/jeeemi.v7i4.795

[10] R. Kala, R. Chandrasekaran, A. Ahilan, and P. Jayapriya, "Brain Magnetic Resonance Image Inpainting via Deep Edge Region-based Generative Adversarial Network," *Journal of Electrical Engineering & Technology*, pp. 1-12, 2024.

[11] Z. Li, J. Liu, J. Zheng, L. Li, Y. Fu, and Z. Yang, "White Matter-Gray Matter Correlation Analysis Based on White Matter Functional Gradient," *Brain Sciences*, vol.15, no. 1, pp. 26, 2024.

[12] A.J. Thottupattu, J. Sivaswamy, B. Holla, and J. Saini, "Understanding Brain Aging Across Populations: A Comprehensive Framework for Structural Analysis," 2024.

[13] B. T. Monisha, C. Divya, and N. Muthukumaran, "Computerized Diagnosis of Diabetic Retinopathy based on Deep Learning Techniques," *International Conference on Applied Artificial Intelligence and Computing (ICAAIC)*, pp. 331-338, 2022.

[14] H. Kebiri, A. Gholipour, R. Lin, L. Vasung, C. Calixto, Ž. Krsnik, D. Karimi, and M.B. Cuadra, "Deep learning microstructure estimation of developing brains from diffusion MRI: a newborn and fetal study," *Medical Image Analysis*, vol. 95, pp. 103186, 2024.

[15] Y. Xu, R. Quan, W. Xu, Y. Huang, X. Chen, and F. Liu, "Advances in medical image segmentation: a comprehensive review of traditional, deep learning and hybrid approaches," *Bioengineering*, vol. 11, no. 10, pp. 1034, 2024.

[16] J. Lee, M. Lee, J. Lee, R.E. Kim, S.H. Lim, and D. Kim, "Fine-grained brain tissue segmentation for brain modeling of stroke patient," *Computers in Biology and Medicine*, vol. 153, pp.106472, 2023.

[17] Z. Lai, L.C. Oliveira, R. Guo, W. Xu, Z. Hu, K. Mifflin, C. Decarli, S.C. Cheung, C.N. Chuah, and B.N. Dugger, "BrainSec: automated brain tissue segmentation pipeline for scalable neuropathological analysis," *IEEE Access*, vol. 10, pp. 49064-49079, 2022.

[18] V.M. Rao, Z. Wan, S. Arabshahi, D.J. Ma, P.Y. Lee, Y. Tian, X. Zhang, A.F. Laine, and J. Guo, "Improving across-dataset brain tissue segmentation for MRI imaging using transformer," *Frontiers in Neuroimaging*, vol. 1, pp. 1023481, 2022.

[19] M. Veluchamy, and B. Subramani, "Brain tissue segmentation for medical decision support systems," *Journal of Ambient Intelligence and Humanized Computing*, vol. 12, no. 2, pp.1851-1868, 2021.

[20] S.V. Aruna Kumar, E. Yaghoubi, and H. Proença, "A fuzzy consensus clustering algorithm for MRI brain tissue segmentation," *Applied Sciences*, vol. 12, no. 15, pp. 7385, 2022.

[21] S.T. Mhlanga, and S. Viriri, "Deep learning techniques for isointense infant brain tissue segmentation: a systematic literature review," *Frontiers in Medicine*, vol. 10, pp. 1240360, 2023.

[22] X. Fan, S. Shan, X. Li, J. Li, J. Mi, J. Yang, & Y. Zhang, "Attention-modulated multi-branch convolutional neural networks for neonatal brain tissue segmentation," *Computers in Biology and Medicine*, vol. 146, pp. 105522, 2022.

[23] C. Wu, Z. Feng, H. Zhang, and H. Yan, "Graph neural network and superpixel based brain tissue segmentation," In 2022 *International Joint Conference on Neural Networks (IJCNN)*, pp. 01-08, 2022.

[24] Z. Deng, and J. Campbell, Sparse Mixture-of-Experts for Non-Uniform Noise Reduction in MRI Images. *arXiv preprint arXiv:2501.14198*, 2025.

[25] D.R. Ningsih, "Improving retinal image quality using the contrast stretching, histogram equalization, and CLAHE methods with median filters," *International Journal of Image, Graphics and Signal Processing*, vol. 14, no. 2, pp. 30, 2020.

[26] F. Wu, W. Yang, L. Xiao, and J. Zhu, "Adaptive wiener filter and natural noise to eliminate adversarial perturbation," *Electronics*, vol. 9, no. 10, pp. 1634, 2020.

[27] T.S. Priya, and T. Ramaprabha, "Resnet based feature extraction with decision tree classifier for classificaton of mammogram images," *Turkish Journal of Computer and Mathematics Education*, vol. 12, no. 2, pp. 1147-1153, 2021.

[28] M. Behzadpour, B.L. Ortiz, E. Azizi, and K. Wu, Breast tumor classification using efficientnet deep learning model. *arXiv preprint arXiv:2411.17870*. 2024.

[29] S. Shetty, W. Talaat, N. Al-Rawi, S. Al Kawas, M. Sadek, M. Elayyan, K. Gaballah, S. Narasimhan, I. Ozsahin, D.U. Ozsahin, and L.R. David, "Accuracy of deep learning models in the detection of accessory ostium in coronal cone beam computed tomographic images," *Scientific Reports*, vol. 15, no. 1, pp. 8324, 2025.

[30] O. Ayana, D.F. Kanbak, and M.K. Keles, "BSO: Binary Sailfish Optimization for feature selection in sentiment analysis," *An International Journal of Optimization and Control: Theories & Applications*, vol. 15, no. 1, pp. 50-70, 2025.

[31] A.V. Jonnalagadda, and H.A. Hashim, "SegNet: A segmented deep learning based Convolutional Neural Network approach for drones wildfire

Manuscript received March 29, 2024; Revised August 10, 2025; Accepted September 5, 2025; date of publication September 8, 2025
Digital Object Identifier (**DOI**): https://doi.org/10.35882/jeeemi.v7i4.795

detection," *Remote Sensing Applications: Society and Environment*, vol. 34, pp. 101181, 2024.

[32] R. Su, J. Liu, D. Zhang, C. Cheng, and M. Ye, "Multimodal glioma image segmentation using dual encoder structure and channel spatial attention block," *Frontiers in Neuroscience*, 14, pp. 586197, 2020.

[33] T. Shan, and J. Yan, "SCA-Net: A spatial and channel attention network for medical image segmentation," *IEEE Access*, vol. 9, pp.160926-160937, 2021.

[34] Alqhtani, S.M., Soomro, T.A., Shah, A.A., Memon, A.A., Irfan, M., Rahman, S., Jalalah, M., Almawgani, A.H. and Eljak, L.A.B., 2024. Improved brain tumor segmentation and classification in brain MRI with FCM-SVM: a diagnostic approach. IEEE Access, 12, pp.61312-61335.

[35] Almufareh, M.F., Imran, M., Khan, A., Humayun, M. and Asim, M., 2024. Automated brain tumor segmentation and classification in MRI using YOLO-based deep learning. IEEE Access, 12, pp.16189-16207.

[36] U. Jain, A. Mirzaei, and I. Gilitschenski, "GaussianCut: Interactive segmentation via graph cut for 3D Gaussian Splatting," In *The Thirty-eighth Annual Conference on Neural Information Processing Systems*, 2024.

[37] Y. Huang, "Evaluating FCN and SegNet for Brain Tumor Segmentation," In *2024 IEEE 2nd International Conference on Electrical, Automation and Computer Engineering (ICEACE)*, pp. 212-216, 2024.

[38] J. Jayapradha, S.C. Haw, N. Palanichamy, S.K. Thillaigovindhan, and M. Al-Tarawneh, "Lung tumor segmentation in medical imaging using U-NET," *Journal of Informatics and Web Engineering*, vol. 4, no. 1, pp. 140-151, 2025.

[39] V.L. Miranda, J.P. Oliveira-Correia, C. Galvão, M.T. Obara, A.T. Peterson, and R. Gurgel-Gonçalves, "Automated identification of Chagas disease vectors using AlexNet pre-trained convolutional neural networks," *Medical and Veterinary Entomology*, vol. 39, no. 2, pp.291-300, 2025.

[40] Y. Chen, S.A. Sharifuzzaman, H. Wang, Y. Li, L.M. Dang, H.K. Song, and H. Moon, "Deep learning based underground sewer defect classification using a modified RegNet," *Comput. Mater. Contin*, vol. 75, pp. 5455-5473, 2023.

[41] S.H. Chen, Y.L. Wu, C.Y. Pan, L.Y. Lian, and Q.C. Su, "Breast ultrasound image classification and physiological assessment based on GoogLeNet," *Journal of Radiation Research and Applied Sciences*, vol. 16, no. 3, pp. 100628, 2023.

[42] E. Elfatimi, R. Eryigit, and L. Elfatimi, "Beans leaf diseases classification using mobilenet models," *Ieee Access*, vol. 10, pp. 9471-9482, 2022.

Author Biography

Athur Shaik Ali Gousia Banu Assistant Professor at Muffakham Jah College of Engineering & Technology (MJCET), is a highly accomplished academician with over 30 years of teaching experience in Computer Science, Information Technology, and Management. Holding a B. Tech (AMIE) in CSE, M. Tech (CSE), MBA (Systems), and a Ph.D. in MIS, she is currently pursuing her second Ph.D. in CSE. She is ratified by both Osmania University and JNTUH and has been recognized with the Ideal Teaching Award Programme (ITAP) in 2022. Her teaching spans from polytechnic institutions to undergraduate and postgraduate levels, covering B. Tech, M. Tech, MBA, MCA, and M. Phil. programs. Dr.

Sumit Hazra received his Ph.D. in Computer Science and Engineering from National Institute of Technology (NIT) Rourkela, Odisha in 2023. He received his M. Tech degree in Computer Science and Engineering from VIT University, Vellore, India. He received his B. Tech Computer Science and Engineering degree from WBUT (currently MAKAUT). He works as an Assistant Professor & AI/ML Research Group Head in the Department of Computer Science and Engineering at Koneru Lakshmaiah Education Foundation, Hyderabad. IEEE Transactions on Cybernetics, Biomedical Signal Processing & Control, Cognitive Neurodynamics, Scientific Reports, etc. He is also a member of the IEEE Professional Body. He has organized several FDPs and workshops, and has been an active member of various committees for several International Conferences. His research interests include Gait Analysis, Cognitive Science, Artificial Intelligence, Pattern Recognition, Computer Vision, etc.

Manuscript received March 29, 2024; Revised August 10, 2025; Accepted September 5, 2025; date of publication September 8, 2025
Digital Object Identifier (**DOI**): https://doi.org/10.35882/jeeemi.v7i4.795